AN IMPROVED COHESIVE ZONE MODEL VIA SELECTIVE ACTIVATION

William M. Peterson[1] and Douglas S. Cairns[1]

[1]Mechanical and Industrial Engineering Department, Montana State University
P.O. Box 173820, Bozeman, MT, USA
Email: william.peterson@msu.montana.edu, web page: http://www.coe.montana.edu

Keywords: Cohesive Zone Model; Crack propagation; Multipoint constraint; Selective activation

ABSTRACT

We present a method for fracture simulations on a standard mesh that combines advantages of both intrinsic and extrinsic cohesive zone models. We demonstrate that the method results in an initially rigid cohesive zone in which intrinsic cohesive elements remain dormant until needed during the course of the analysis. Once a critical region in the mesh is identified, cohesive elements may be selectively reactivated in a logical and consistent manner. The method successfully alleviates the problem of artificial compliance inherent to the intrinsic approach and minimizes the number of additional degrees of freedom (DOF) necessary to track crack growth, and in many cases reducing the total computational time. Indeed, prior to fracture the number of active DOF is exactly equal to that of a conventional mesh, and the solution yields identical results. However, unlike the typical adaptive extrinsic approach, a framework designed to handle adaptive updates to the mesh topology are unnecessary and the solution proceeds without interruption. In addition, we may later deactivate sufficiently relaxed cohesive elements that have not been fully damaged once a crack tip has propagated away from a previously critical region.

1 INTRODUCTION

Material fracture and failure can be modeled in the finite element method using cohesive interface elements (CIEs) that represent crack openings by localizing displacement jumps at inter-element boundaries. The crack opening is then governed by a traction-separation law (TSL) which describes the development of cohesive tractions across the interface as a function of the interfacial separation. Typically, cohesive elements are placed within a mesh along an expected fracture path, forming a so-called cohesive zone through which cracks may propagate. The foremost example is the analysis of delamination in composite laminates which may be accurately modeled by placing CIEs at the ply boundaries [1].

Rather than predefining the fracture path, a more general approach is to insert CIEs between all elements within a region of interest such that all of the element boundaries become potential fracture paths, as indicated in Fig X. Because the CIEs exist within the mesh prior to obtaining the solution, this approach is referred to as the intrinsic cohesive model. Pioneered by Ortiz and Suresh [3] and Xu and Needleman [4], the main advantage of the full intrinsic model is that the initial crack site as well as the fracture path need not be known *a priori*. Multiple cracks, crack interaction, and fragmentation are naturally permitted. However, despite this versatility the full intrinsic model is apparently absent from commercial finite element codes and is not commonly seen in the literature. This is perhaps due to a few shortcomings of the intrinsic approach, which include (1) an artificial added compliance of the model due to the necessity of an initial elastic response of the cohesive elements, (2) the large number of additional degrees of freedom (DOF) that are a result of node duplication that is necessary during mesh splitting and CIE insertion, and (3) the potential fracture paths are limited to inter-element boundaries, and are therefore inherently mesh-dependent. In most cases, the artificial compliance issue is the most difficult to overcome. To compensate, the analyst may choose to reduce artificial compliance by assuming very large values for the initial elastic "penalty" stiffness, such that the interface becomes nearly rigid prior to the onset of damage and softening. Unfortunately, this leads to ill-conditioning of

the global stiffness matrix and numerical non-convergence. In practice, a suitable value for the penalty stiffness in intrinsic models is often only found by iteration. Crack growth mesh dependence may also be acceptably reduced by using a sufficiently refined and unstructured mesh which provides a variety of potential fracture paths, and performing a parametric study over a reasonable number of mesh variants. As usual, there is a trade-off between acceptable computational expense and accuracy.

In a second approach, often referred to as an initially-rigid or extrinsic cohesive model, CIEs are adaptively inserted wherever required as the solution progresses [4]. This approach reduces the issue of artificial compliance while preventing CIE insertion (along with the corresponding increase in the number of active DOF) if damage is not indicated. However, continual remeshing operations are often computationally inefficient, and tend to require sophisticated data storage and transfer routines.

2 SELECTIVELY ACTIVATED COHESIVE ZONE MODEL

In this section we describe a new approach that combines advantages of both intrinsic and extrinsic models by selectively activating cohesive elements using controllable multipoint constraints (MPCs). Similar to the intrinsic approach, we begin by inserting cohesive elements at every inter-element boundary in the initial mesh during model preprocessing. This is accomplished by using a fast and robust in-house remeshing code we have developed for this purpose, which operates on the nodal coordinate and element connectivity tables that are commonly produced using standard finite element mesh generators. Each element of the mesh is separated from all adjacent elements, forming a domain of fully discontinuous elements with unique nodes and surfaces. Note that each “parent” node is duplicated as many times as it is shared by elements in the original mesh, and each new “child” node shares the exact location in space as the parent node. Zero-thickness CIEs are then inserted at all inter-element boundaries. Once remeshing is complete, a typical intrinsic CZM has been generated, as shown in Fig. 1. Of course, in many practical fracture analyses this process results in a substantial increase in the number of nodes and associated DOF.

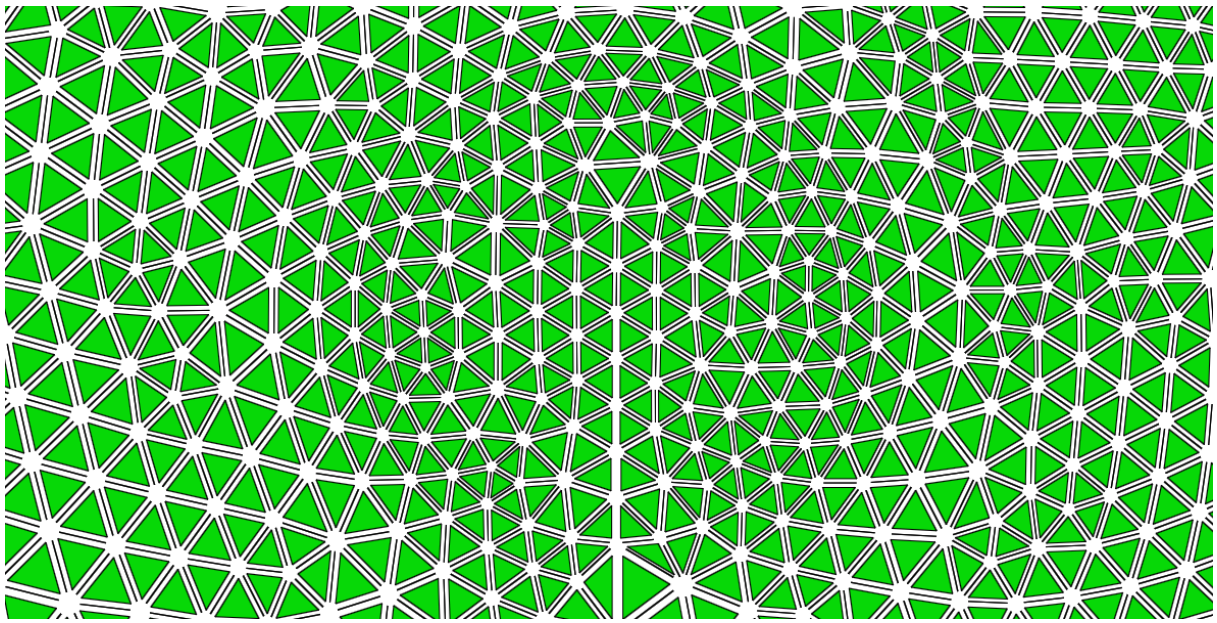

Figure 1: Example Intrinsic Cohesive Zone Mesh. Continuum elements are shrunk in order to clarify the position of the inserted CIEs. Note that a crack is shown at the center, where CIEs are not present.

Using element adjacency information obtained during the remeshing step, we then define node-to-node linear master-slave MPCs such that the superposed nodes of adjacent elements are exactly constrained to prevent relative displacements via a congruent transformation (Fig. 2). The eliminated slave DOF are retained so that they may be reactivated as needed during the analysis; however, the number of active DOF is returned to that of the original mesh by virtue of the method. Each intrinsic cohesive element enters a “dormant” state and has no effect on the response of the structure.

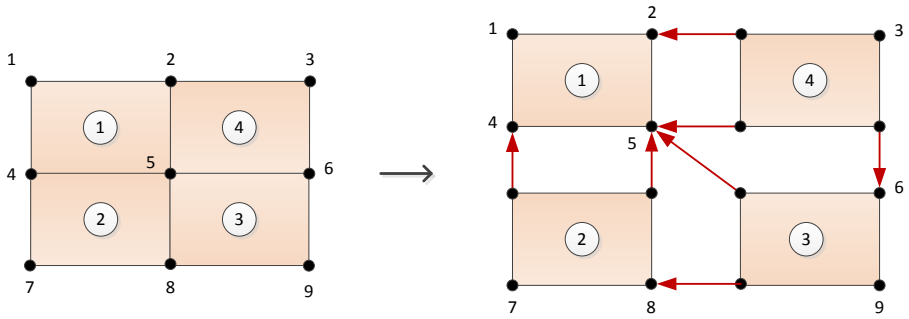

Figure 2: Mesh splitting and node-to-node multipoint constraints. The location of the original node numbers is shown on the split mesh. The original nodes are retained as master nodes in order to simplify the transfer of boundary conditions defined on the original mesh.

During the analysis, at the conclusion of each converged increment the solution is investigated to identify critical regions in the mesh. Constraints may then selectively deactivated wherever a damage criterion is satisfied. Subsequent inter-element displacement and damage evolution is then governed by an appropriate TSL. In other words, the solution continues to the next increment without interruption even as cohesive elements and DOF are reintroduced into the model.

We have implemented a version of the proposed model via a user subroutine coupled with the commercial finite element code Abaqus/Standard (implicit). The MPC, UFIELD, and URDFIL subroutines allow access to certain key functionalities. We enable access to shared variables that cannot otherwise be communicated through the subroutine arguments through a Fortran Module. In a future publication we will describe a new implementation of the proposed model using the UEL subroutine.

3 PATCH TEST COMPARISON

In the following section, the 2D finite element patch test is adapted in order to illustrate the differences between a conventional (continuum element only) mesh, an intrinsic cohesive zone model (CZM), and the selectively activated MPC-based cohesive zone model (MCZM). This example serves to clearly demonstrate that even using very large initial penalty stiffness values, K, the CZM fails to calculate the correct displacement solution; consequently, the use of a large value for K will fail to preserve the correct element-local response (for example, stress) in the intrinsic model.

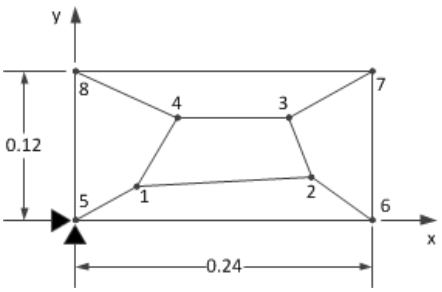

Figure 3. Typical 5-element membrane patch test. All units in meters

Consider the 5-element membrane 2D patch test in Fig. 3. The mesh shown consists of linear plane-strain elements where the Young's modulus and Poisson's ratio are E=1.0 MPa and ν= 0.25. All exterior nodes (Nodes 5-8) are subjected to the prescribed displacement field:

$$U_x = 10^{-3}(x + 0.5y) \quad (1a)$$

$$U_y = 10^{-3}(0.5x + y) \quad (1b)$$

Therefore, the boundary conditions at the exterior nodes are:

Node 5: $U_x = 0$ $U_y = 0$

Node 6:	$U_x = 0.24 \cdot 10^{-3} m$	$U_y = 0.12 \cdot 10^{-3} m$
Node 7:	$U_x = 0.3 \cdot 10^{-3} m$	$U_y = 0.24 \cdot 10^{-3} m$
Node 8:	$U_x = 0.06 \cdot 10^{-3} m$	$U_y = 0.12 \cdot 10^{-3} m$

For a mesh of linear elements, the patch test is passed if the displacement of the interior nodes (Nodes 1-4) match the prescribed displacement field given in Eq. (1). The analytical reference solution for the displacement of the interior nodes is:

Node 1:	$U_x = 0.05 \cdot 10^{-3} m$	$U_y = 0.04 \cdot 10^{-3} m$
Node 2:	$U_x = 0.195 \cdot 10^{-3} m$	$U_y = 0.12 \cdot 10^{-3} m$
Node 3:	$U_x = 0.2 \cdot 10^{-3} m$	$U_y = 0.16 \cdot 10^{-3} m$
Node 4:	$U_x = 0.12 \cdot 10^{-3} m$	$U_y = 0.12 \cdot 10^{-3} m$

In Fig. 4, the construction and final active DOF for each model is illustrated. In this example, we look at results from several different intrinsic models with increasing penalty stiffness values (see Table 1). Note that the cohesive element stiffness chosen for the MCZM is arbitrary for this example, since the cohesive elements are effectively condensed from the problem and the MPCs are not released. The displacement field plots for example solutions are shown in Figs. 5-8 (for clarity, the cohesive elements are not visualized). From these figures, it is clear that the conventional and MCZM meshes pass the displacement patch test. Of course, displacement continuity must be perfectly satisfied using the master-slave MPC approach. On the other hand, the intrinsic cohesive mesh exhibits severe discontinuities, even without permitting damage initiation and for very high penalty stiffness.

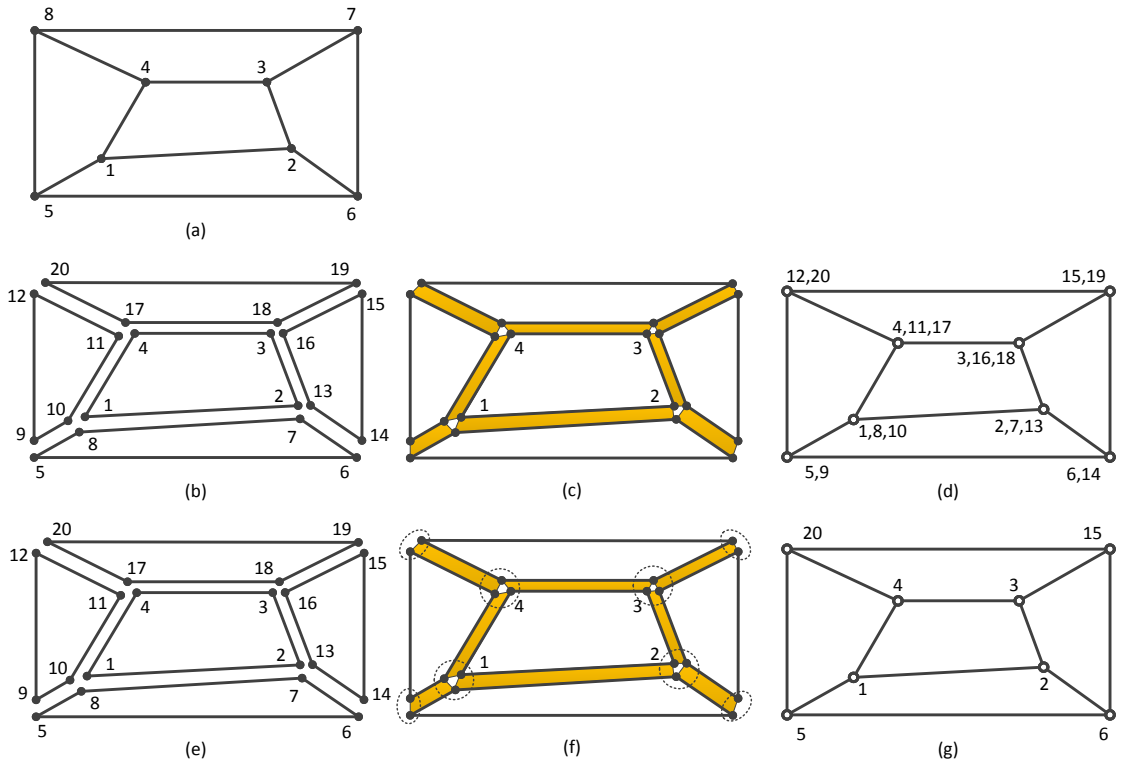

Figure 4. Construction of patch test models. Top (a): conventional mesh; Middle (b-c): intrinsic CZM; Bottom (e-f): MCZM. Gaps between elements are shown only for clarity. Cohesive elements are shaded. Only nodes with active DOF are numbered by the right-most figure in each row. Note that the interior element has the same nodal numbering in each model.

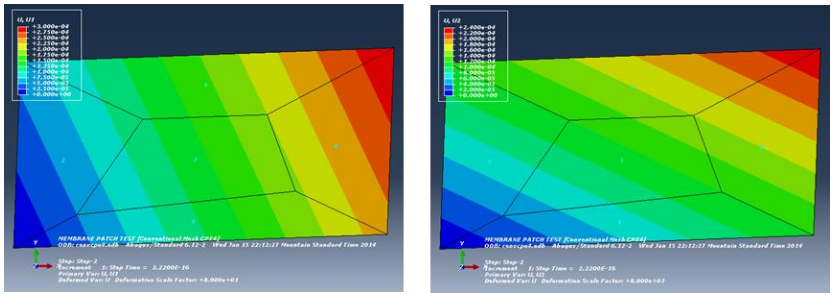

Figure 5. Conventional mesh patch test: displacement. Left: U1, right: U2. Scale factor=80.

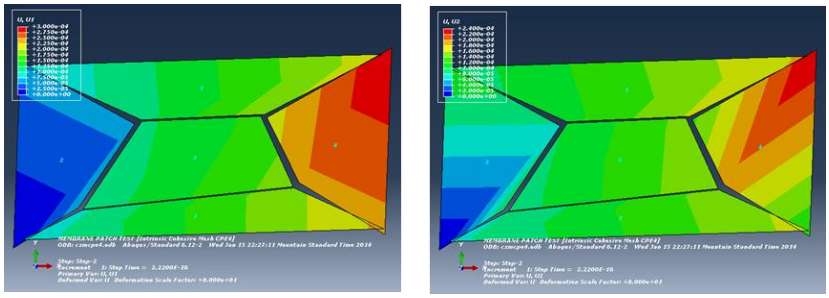

Figure 6. Intrinsic mesh (K=10·E) patch test: displacement. Left: U1, right: U2. Scale factor=80.

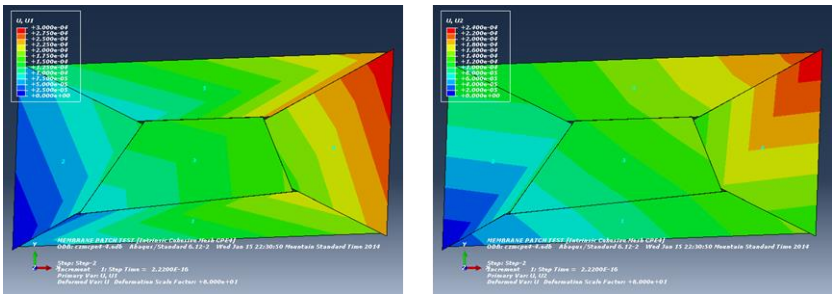

Figure 7. Intrinsic mesh (K=10^4·E) patch test: displacement. Left: U1, right: U2. Scale factor=80.

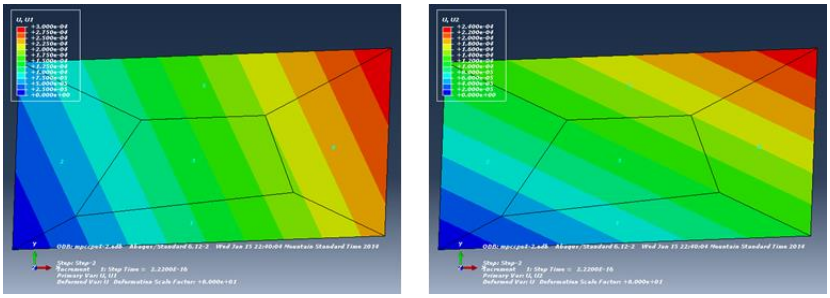

Figure 8. MCZM patch test: displacement. Left: U1, right: U2. Scale factor=80.

#	Model Description	Penalty Stiffness, K
1	Conventional (Linear Plane Strain CPE4) Mesh	NA
2	Intrinsic Cohesive Mesh	$10^1 \cdot E$
3	Intrinsic Cohesive Mesh	$10^2 \cdot E$
4	Intrinsic Cohesive Mesh	$10^3 \cdot E$
5	Intrinsic Cohesive Mesh	$10^4 \cdot E$
6	MCZM	$10^1 \cdot E$

Table 1. Models used in the patch test comparison

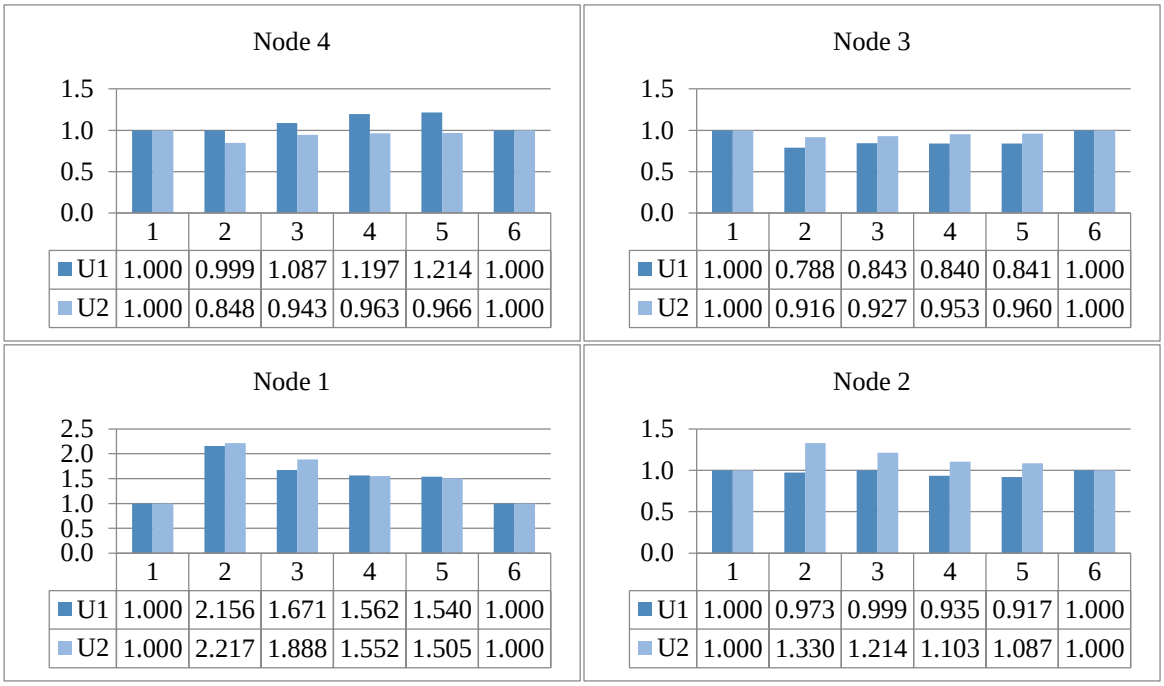

Figure 9: Displacement solution at nodes 1-4 of the interior element, normalized to the analytical solution. Note that an exact solution is represented by a value of "1.0". See Table 1 for a description of Models 1-6.

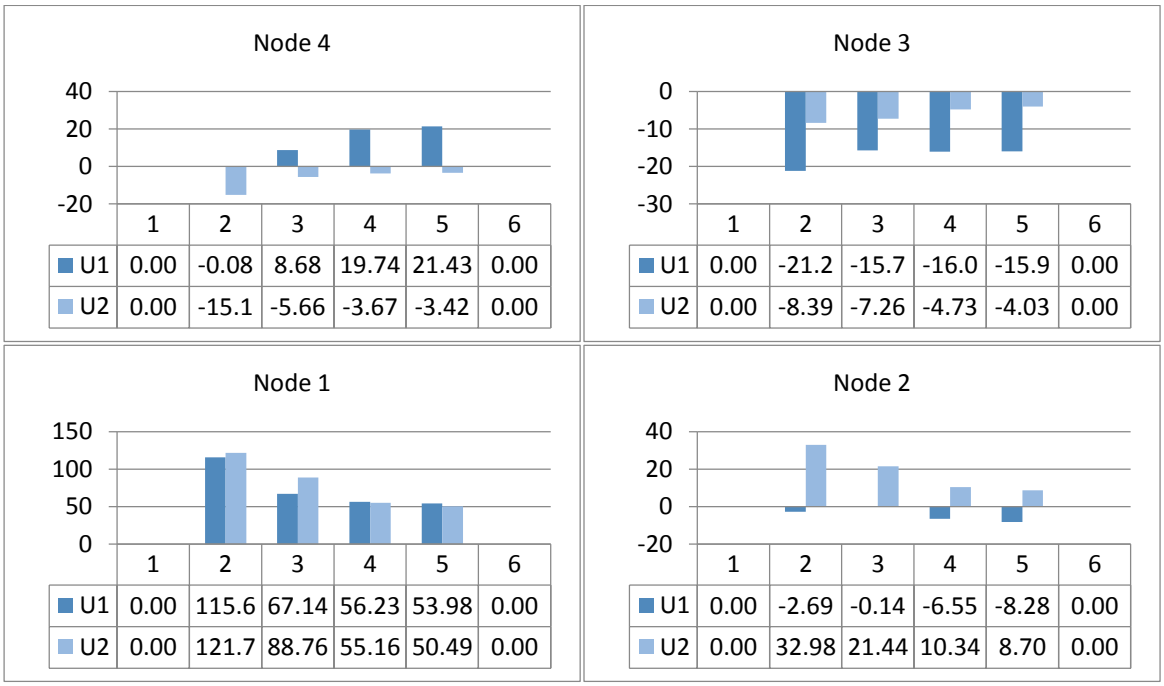

Figure 10: Percent error in the displacement solution at nodes 1-4 of the interior element. Note that an exact solution is represented by a value of '0'. See Table 1 for a description of Models 1-6.

In Fig. 9, the displacements of the interior nodes are shown, normalized to the exact solution. Nodes are numbered as given in Fig. 4, and models are numbered as in Table 1. It can be seen that the conventional and MCZM meshes arrive at the correct values, while the intrinsic mesh fails to reach the correct local solution even for very large penalty stiffness, K. We can also note that as K increases (by 4 orders of magnitude), there does not appear to be any general improvement in the solution computed

with the intrinsic mesh. This is perhaps made more evident in Fig. 10, where the percent errors for the interior node displacements are shown.

4 DRILLED PLATE VALIDATION TEST

We take an interesting problem by Ingraffea and Grigoriu [6], similar to that of Bittencourt et al. [7], as a test of the selectively activated CZM. In their work, Plexiglas (PMMA) specimens were tested in 3-point bending under the influence of three drilled holes, and the resulting crack path was investigated for various initial crack locations and lengths. We analyze only one of the crack geometries studied by them, and determine the resulting fracture path for three values of the cohesive fracture energy. A simple displacement-controlled boundary condition was applied to the center of the top edge. The geometry and isotropic material properties are illustrated in Fig. 11. A standard 2D cohesive element available in Abaqus was used without modification of the intrinsic TSL with an initial stiffness of 10·E (in a future publication we will demonstrate an alternative UEL-based cohesive element with an extrinsic TSL). Multipoint constraints were released at an effective Mises stress of $\sigma_{rel} = 0.95*\sigma_{max}$. The mesh consisted of 58875 nodes with 19625 3-node linear triangles (CST) and 29223 4-node bilinear cohesive elements. Solutions were obtained between 45-60 mins using 2 cores on a modest Intel i3 with 6GB RAM running Windows 7.

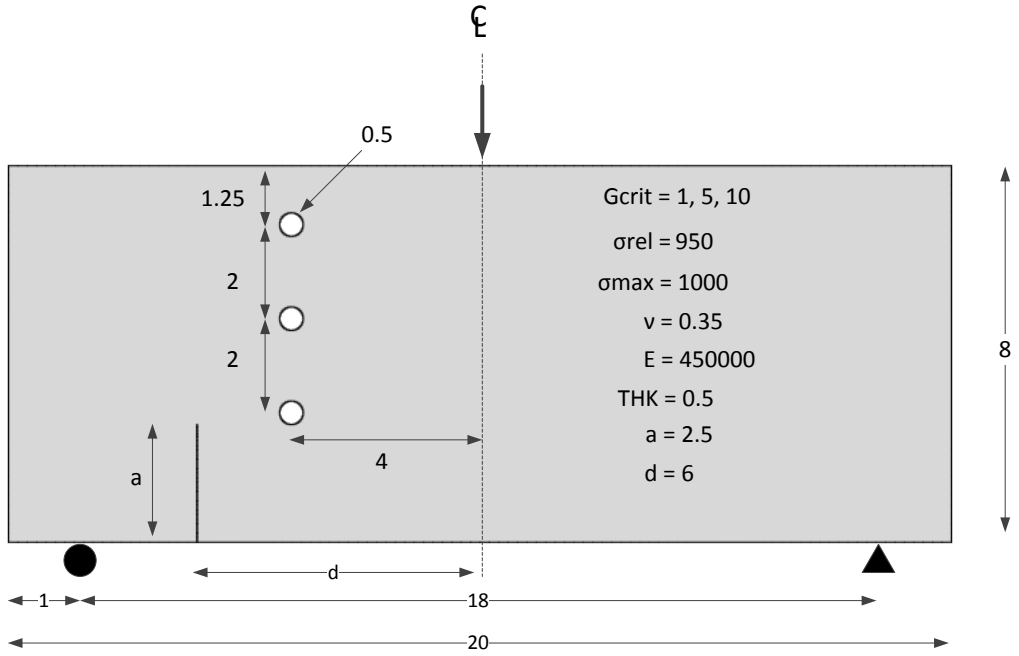

Fig. 11: Ingraffea/Bittencourt's Drilled Plate [6,7]. All dims in inches.

The crack path results are shown in Figs. 12-14. Dark lines or dots on the interior of the model indicate the presence of a free surface – i.e. an MPC has been released. The results are encouraging, although not exactly the same as in [6]. This discrepancy is partly due to the restriction that crack growth must occur along inter-element boundaries, and partly a result of the simple displacement control method used in our analysis. For the same mesh, we note the change in the crack path as the critical fracture energy increases.

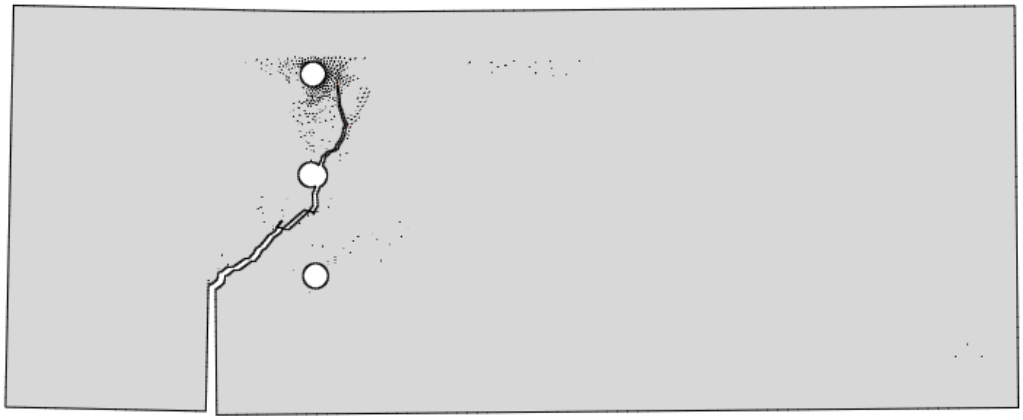

Fig. 12: Selectively Activated CZM; G_{crit} = 10. Scale factor=1.

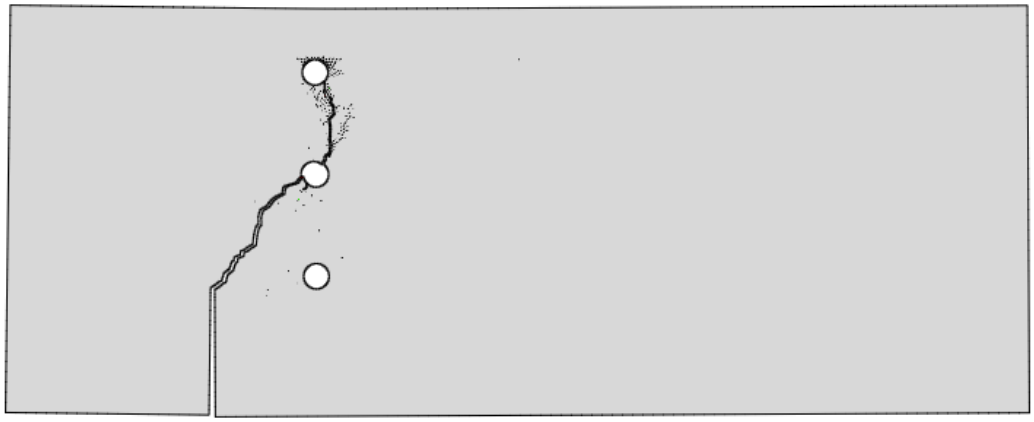

Fig. 13: Selectively Activated CZM; G_{crit} = 5. Scale factor=1.

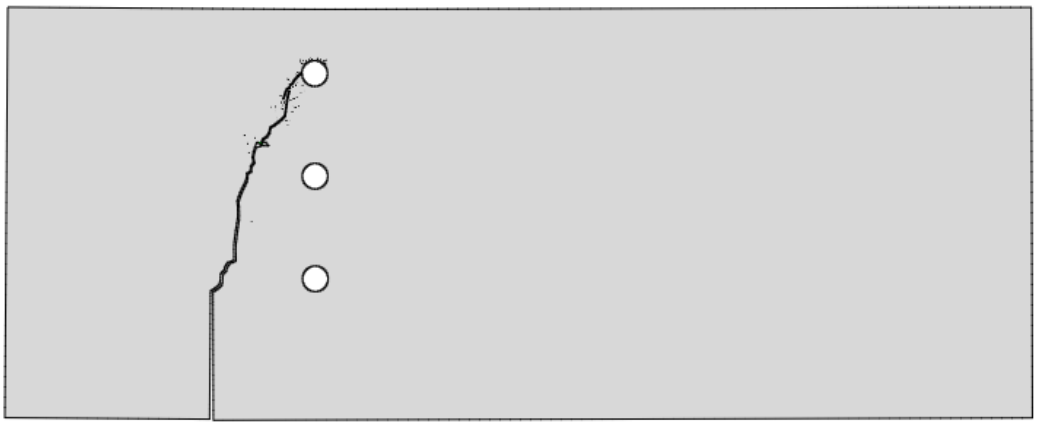

Fig. 14: Selectively Activated CZM; G_{crit} = 1. Scale factor=1.

5 CONCLUSIONS

The cohesive zone model is a versatile tool for modeling crack initiation and propagation under complex loading conditions, but both intrinsic and extrinsic approaches suffer from some drawbacks. The selective activation of intrinsic cohesive elements appears to be a natural extension that removes or lessens these issues by (1) alleviating the effect of artificial compliance, (2) minimizing the number of DOF in the system matrix while retaining eliminated DOF for reactivation as needed, and (3) utilizing dormant cohesive elements that are selectively reactivated at inter-element boundaries only as

needed by the analysis, rather than by interrupting the solution in order to perform adaptive remeshing and element insertion. The method is quite flexible, as well, permitting the reactivation of MPCs upon sufficient relaxation of the undamaged CIEs in a cohesive zone after a crack has passed through a formerly critical region. Continued development will be reported in future publications.

REFERENCES

[1] Alfano, G., and Crisfield, M.A., "Finite element interface models for the delamination analysis of laminated composites: mechanical and computational issues", International Journal for Numerical Methods in Engineering, Vol. 50, 2001, pp. 1701-1736.
[2] Ortiz, M., and Suresh, S., "Statistical properties of residual stresses and intergranular fracture in ceramic materials", Journal of Applied Mechanics, Vol. 60, 1993, pp. 77-84.
[3] Xu, X.-P, and Needleman, A., "Numerical simulations of fast crack growth in brittle solids", Journal of the Mechanics and Physics of Solids, Vol. 42, 1994, pp. 1397-1434
[4] Camacho, G. T.; Ortiz, M., "Computational modelling of impact damage in brittle materials", International Journal of Solids and Structures, 1996, Vol. 33; pp. 2899-2938.
[5] Abaqus User's Manual, Ver. 6.12, Simulia, 2012.
[6] Ingraffea, A.R; Grigoriu, M., "Probabilistic fracture mechanics; A validation of predictive capability", AFOSR Final Report, 1990.
[7] Bittencourt, T.N.; Wawrzynek, P.A.; Ingraffea, A.R.; "Quasi-automatic simulation of crack propagation for 2D LEFM problems", Engineering Fracture Mechanics, 1995, Vol. 55, No. 2; pp. 321-334.